

Article

# The Large-Scale Preparation and Optical Properties of MoS<sub>2</sub>/WS<sub>2</sub> Vertical Hetero-Junction

Tao Han, Hongxia Liu , Shulong Wang , Shupeng Chen and Kun Yang 

Key Laboratory for Wide-Bandgap Semiconductor Materials and Devices of Education, the School of Microelectronics, Xidian University, Xi'an 710071, China; taohan373@gmail.com (T.H.); spchen@xidian.edu.cn (S.C.); kuny2019@163.com (K.Y.)

\* Correspondence: hxliu@mail.xidian.edu.cn (H.L.); slwang@xidian.edu.cn (S.W.);

Tel.: +86-130-8756-8718 (H.L.); +86-150-9115-4611 (S.W.)

Academic Editors: Magnus Willander and Peng Si

Received: 14 March 2020; Accepted: 16 April 2020; Published: 17 April 2020



**Abstract:** A variety of hetero-junctions can be constructed to form the basic structural units in the different optoelectronic devices, such as the photo-detectors, solar cells, sensors and light-emitting diodes. In our research, the large-area high-quality MoS<sub>2</sub>/WS<sub>2</sub> vertical hetero-junction are prepared by the two-step atmospheric pressure chemical vapor deposition (APCVD) methods and the dry transfer method, and the corresponding optimal reaction conditions of MoS<sub>2</sub>/WS<sub>2</sub> vertical hetero-junction are obtained. The morphology, composition and optical properties of MoS<sub>2</sub>/WS<sub>2</sub> vertical hetero-junction are systematically characterized by the optical microscopy, Raman spectroscopy, photoluminescence spectroscopy, atomic force microscopy and the field emission scanning electron microscopy. Compared to the mechanical transfer method, the MoS<sub>2</sub>/WS<sub>2</sub> vertical hetero-junction sample obtained by the APCVD and dry transfer methods have lower impurity content, cleaner interfaces and tighter interlayer coupling. Besides, the strong interlayer coupling and effective interlayer charge transfer of MoS<sub>2</sub>/WS<sub>2</sub> vertical hetero-junction are also further studied. The photoluminescence intensity of MoS<sub>2</sub>/WS<sub>2</sub> vertical hetero-junction is significantly reduced compared to the single MoS<sub>2</sub> or WS<sub>2</sub> material. In general, this research can help to achieve the large-scale preparation of various Van der Waals hetero-junctions, which can lay the foundation for the new application of optoelectronic devices.

**Keywords:** MoS<sub>2</sub>/WS<sub>2</sub> vertical hetero-junction; optical properties; Raman spectrum; PL spectrum; AFM; SEM

## 1. Introduction

The electronic chips integration increase with the development of modern semiconductor technology, and the volume of devices is becoming smaller, with the preparation processes becoming more complex [1–3]. The size of conventional Si-based CMOS devices has approached the limit, so researchers turn their attention to the two-dimensional transition metal dichalcogenides (2D TMDs) materials with single atomic layers. However, there are some limitations in the application of the single two-dimensional materials. The single h-BN material cannot be used in the devices alone, due to its wide band gap [4]. Additionally, the exposed BP is easily oxidized in the air, which would lead to the degradation of its performance [5]. As we all know, different two-dimensional materials have different energy band structures and band gaps. To further investigate the intrinsic properties of two dimensional materials and expand the application fields, the two dimensional hetero-junction materials can concentrate the advantages of two materials together to achieve the precise adjustment of the band gap, and it can also finely regulate the physical properties of the single materials. The advantage of Van der Waals (VDWs) atomic level hetero-junction has the convenience of modular combination, compared with the conventional hetero-junction. In other words, the atomic layer materials could

be combined to prepare the hetero-junctions at will, which does not need to consider the lattice matching [6,7]. The corresponding hetero-junctions can be formed by stacking these atomic layer materials, which would show some properties not available in the single material. Besides, it can also achieve complementary properties.

The 2D TMD materials have large band gaps of a two-dimensional structure from the visible light to the near-infrared spectrum, adjustable carrier mobility, and electronic and optical characteristics related to the layer number [8,9]. It is these excellent characteristics that make them show great potential in the application of optoelectronic devices, such as the photo detectors [10], and the light emitting diodes [11]. The combination of MoS<sub>2</sub> and WS<sub>2</sub> films can effectively adjust the optical and electrical properties of MoS<sub>2</sub>/WS<sub>2</sub> vertical hetero-junction through interlayer coupling, which would result in effective charge transfer and band structure reorganization. Meanwhile, they have a rich phenomenon of physics and electronics, which can also provide new opportunities for the design of novel electronic devices and photonic devices. In the previous reports, the mechanical stripping and chemical vapor deposition methods are usually used for the controlled and scalable production of the transition metal sulfides and the large-scale synthesis of TMDs with ideal architecture [12,13]. The mechanical exfoliation and directional transfer methods are the most widely used to study the VDWs hetero-structures, but the successful accumulation is accidental, and the methods have lower yield and efficiency [14]. Although some progress has been made in the preparation of TMD hetero-structures by the chemical vapor deposition method (CVD), conventional methods can usually only produce the lateral structures and not vertical hetero-structures. Therefore, there is still a huge challenge in using the existing exfoliation or CVD growth processes to achieve the scalable production of TMDs hetero-junctions with well-controlled structures.

The VDWs hetero-junction can be formed by using mechanical transfer technology to stack the different 2D materials, which has limited stacking orientation control. Compared to the mechanical transfer method, the direct growth of MX<sub>2</sub> hetero-structure by CVD method not only has inherent scalability, but also has a cleaner interface and tighter interlayer coupling [15]. In this paper, the two-step atmospheric pressure chemical vapor deposition (APCVD) and dry transfer methods are used to epitaxially grow WS<sub>2</sub> on MoS<sub>2</sub>, which can prepare the MoS<sub>2</sub>/WS<sub>2</sub> vertical hetero-junction with its clean interface and strong interlayer coupling. The optimal processes' reaction conditions of MoS<sub>2</sub>/WS<sub>2</sub> vertical hetero-junction can also be obtained. Meanwhile, the morphology, composition and optical properties of MoS<sub>2</sub>/WS<sub>2</sub> vertical hetero-junction are systematically characterized by optical microscopy, Raman spectroscopy, photoluminescence (PL) spectroscopy, atomic force microscopy, and field emission scanning electron microscopy. The results shown in this paper can provide effective guidance for future photonic devices, solar cells, photo-detectors, modulators, and storage devices [16].

## 2. The Introduction of Experiment

### 2.1. The Growth Experiments of MoS<sub>2</sub> or WS<sub>2</sub> by APCVD

The sulfur powder, tungsten trioxide, and molybdenum trioxide are respectively used as the sulfur source, tungsten source, and molybdenum source in the MoS<sub>2</sub> or WS<sub>2</sub> materials growth experiment, and the MoS<sub>2</sub> and WS<sub>2</sub> materials are respectively grown on SiO<sub>2</sub>/Si substrates by the atmospheric pressure chemical vapor deposition (APCVD) method. The following are the specific growth processes of single MoS<sub>2</sub> or WS<sub>2</sub> materials [17]. First, the SiO<sub>2</sub>/Si substrates are sequentially put into the absolute ethanol, acetone, and deionized water for 10 minutes, and then washed with the deionized water. Next, the first quartz boat with 0.1 g sulfur powder is put into the low temperature zone of the dual-temperature zone tube furnace. At the same time, the second quartz boat, equipped with 2 mg molybdenum source or tungsten source and the cleaned SiO<sub>2</sub>/Si substrate, is placed in the high temperature zone of the double temperature zone tube furnace, as shown in Figure 1a. Then, the tube furnace is evacuated to the vacuum state (1 Pa) when the vacuum pump is turned on, and then the high purity argon gas is used to fill the entire quartz tube chamber to reach the normal pressure

state (100 KPa). The above operation is repeated three times to eliminate the air of the quartz tube. Subsequently, the heating program of the tube furnace is opened, and the growth temperatures of MoS<sub>2</sub> and WS<sub>2</sub> are respectively set to 720 °C and 800 °C due to the different sublimation points. The temperature of MoO<sub>3</sub> powder increased from 25 °C to 720 °C, which was completed with a rate of 15.8 °C/min for 30 min and in turn 22 °C/min for 10 min. Meanwhile, the temperature of WO<sub>3</sub> powder was increased from 25 °C to 800 °C, and successively heated at a rate of 17.5 °C/min for 30 min and 25 °C/min for 10 min. After the MoO<sub>3</sub> and WO<sub>3</sub> powders completed the first-stage heating, the temperature of sulfur powder increased from 25 °C to 200 °C in 10 min. Besides, the heating time remained unchanged for 10 min under the growth condition, and the flow rate of shielding gas is 35 sccm during the reaction. Finally, the heating program was turned off when the growth of single MoS<sub>2</sub> or WS<sub>2</sub> materials was completed, and the corresponding samples were taken out when the tube furnace was cooled to room temperature.

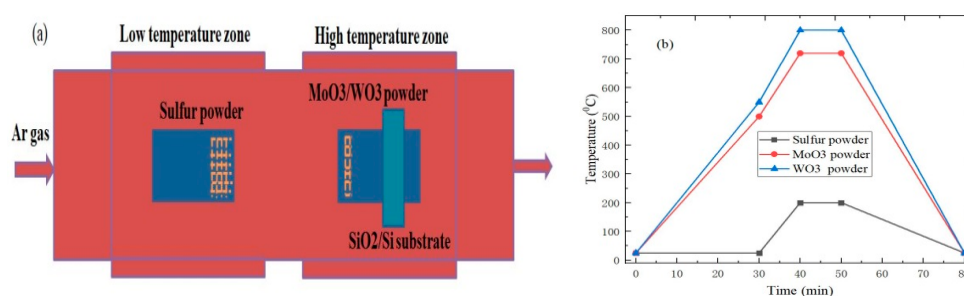


**Figure 1.** (a) Schematic diagram of MoS<sub>2</sub> or WS<sub>2</sub> materials growth experiment by atmospheric pressure chemical vapor deposition (APCVD); (b) The temperature change diagram of MoS<sub>2</sub> or WS<sub>2</sub> materials experiment process by APCVD.

## 2.2. The Preparation Experiment of MoS<sub>2</sub>/WS<sub>2</sub> Vertical Heterojunction

Meanwhile, the preparation processes of the MoS<sub>2</sub>/WS<sub>2</sub> vertical hetero-junction by the dry transfer method are also described in previous work [18]. Based on the previous MoS<sub>2</sub> and WS<sub>2</sub> materials prepared by APCVD, the polymethyl methacrylate (PMMA) liquid was spin-coated on the WS<sub>2</sub> at a speed of 4000 r/s, and annealed at 150 °C for 30 min. Additionally, the PMMA film can be immersed in the NaOH solution (Lingping Chemical Glass Instrument Co., Ltd., Guangzhou, China, 0.1 Mol/L). Then, the PMMA film with WS<sub>2</sub> is floated and transferred to another SiO<sub>2</sub>/Si substrate, by using the transfer platform under the condition of CCD monitoring, which would overlap with the MoS<sub>2</sub>. Finally, the PMMA film is dissolved with acetone, and the MoS<sub>2</sub>/WS<sub>2</sub> vertical hetero-junction can be obtained.

## 2.3. The Characterization of MoS<sub>2</sub>/WS<sub>2</sub> Vertical Heterojunction

The Raman spectrum and PL spectrum of the MoS<sub>2</sub>/WS<sub>2</sub> vertical hetero-junction are systematically analyzed by the LabRam HR Evolution Raman microscopy, equipped with the 532 nm laser under the 1mW laser power, and the laser spot size is 1μm. The high-resolution images can be obtained by using the 50× objective lens, 1800 lines/mm grating and the 500 nm imaging steps [19]. At the same time, the field emission scanning electron microscope (FESEM) and atomic force microscope (AFM) are also used to characterize the surface morphology and thickness of the MoS<sub>2</sub>/WS<sub>2</sub> vertical hetero-junction.

## 3. The Analysis of Characterization Results

In order to obtain better MoS<sub>2</sub>/WS<sub>2</sub> vertical hetero-junction materials, we first need to grow the high-quality large-area single MoS<sub>2</sub> or WS<sub>2</sub> materials by APCVD. Under the optimal growth conditions, the gas concentration and nucleation density of single MoS<sub>2</sub> or WS<sub>2</sub> materials in the tube furnace can achieve the maximum values [20]. The MoS<sub>2</sub>/WS<sub>2</sub> double-layer vertical hetero-junction can be prepared by the two-step APCVD method and the dry transfer processes. At the same time,

the MoS<sub>2</sub>/WS<sub>2</sub> vertical hetero-junction samples are systematically characterized by optical microscopy, Raman spectroscopy, PL spectroscopy, AFM and FESEM. In addition, the surface of WS<sub>2</sub>, MoS<sub>2</sub>, and MoS<sub>2</sub>/WS<sub>2</sub> vertical hetero-junction samples are all uniform triangles with a size of several tens of microns after the corresponding growth reaction, and the color contrast between the samples and SiO<sub>2</sub>/Si substrate is relatively obvious, which can be distinguished by the optical microscope, as shown in Figure 2.

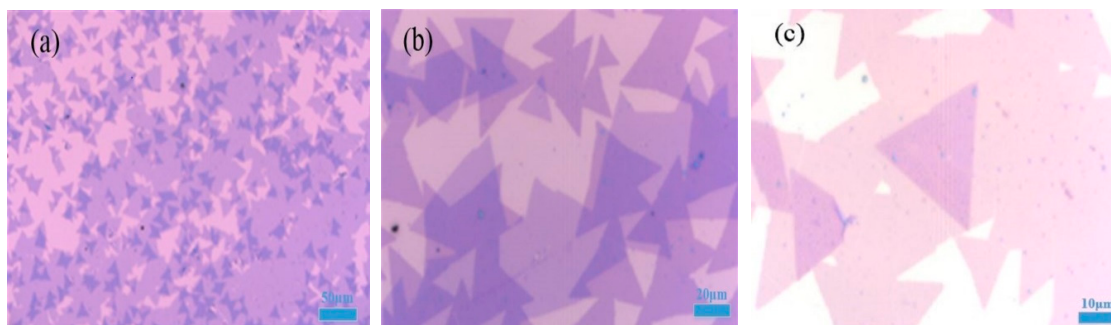


**Figure 2.** Optical microscopy images of MoS<sub>2</sub>/WS<sub>2</sub> vertical hetero-junction at different magnifications (a) 10×; (b) 50×; (c) 100× objectives.

The MoS<sub>2</sub>/WS<sub>2</sub> vertical hetero-junction on SiO<sub>2</sub>/Si substrate can also be observed by the FESEM. It can be found that the size of single WS<sub>2</sub> or MoS<sub>2</sub> materials are respectively 20 μm and 30 μm, and the contrast between single WS<sub>2</sub> or MoS<sub>2</sub> materials and SiO<sub>2</sub>/Si substrate is very uniform.

The reason the overlapping parts are not mixed together to form the WS<sub>2</sub>-MoS<sub>2</sub> lateral hetero-junction is that we have adopted the two-step growth process. The first step is that the WO<sub>3</sub> powder forms the WS<sub>2</sub> crystals during the high temperature (800 °C) reduction and vulcanization process, and the second step is that the MoO<sub>3</sub> forms MoS<sub>2</sub> crystals during the low temperature (720 °C) reduction and vulcanization process. Besides, the PMMA-assisted transfer method is used to transfer the monolayer WS<sub>2</sub> to the monolayer MoS<sub>2</sub> material, and the top WS<sub>2</sub> layer has only 0° and 60° orientation relative to the bottom MoS<sub>2</sub> layer in the red dotted box, which respectively correspond to A-A and A-B stacks [21,22], as shown in Figure 3. Therefore, unlike the traditional CVD method, the injection of Mo into WO<sub>3</sub> to form the lateral MoS<sub>2</sub>-WS<sub>2</sub> mixture is effectively prevented.

Figure 4 shows the AFM images of MoS<sub>2</sub>, WS<sub>2</sub>, and MoS<sub>2</sub>/WS<sub>2</sub> vertical hetero-junction. It can be found by observing the surface morphology and thickness that the thickness of the MoS<sub>2</sub>/WS<sub>2</sub> vertical hetero-junction is about 1.7 nm, as shown in red mark region III. In order to further determine the thickness of single MoS<sub>2</sub> and WS<sub>2</sub> materials, the thickness of region II MoS<sub>2</sub> and region I WS<sub>2</sub> are respectively measured as 0.8 nm and 0.9 nm, which indicates the existence of monolayer WS<sub>2</sub> and monolayer MoS<sub>2</sub>, and the lateral dimension is about 20–30 μm.

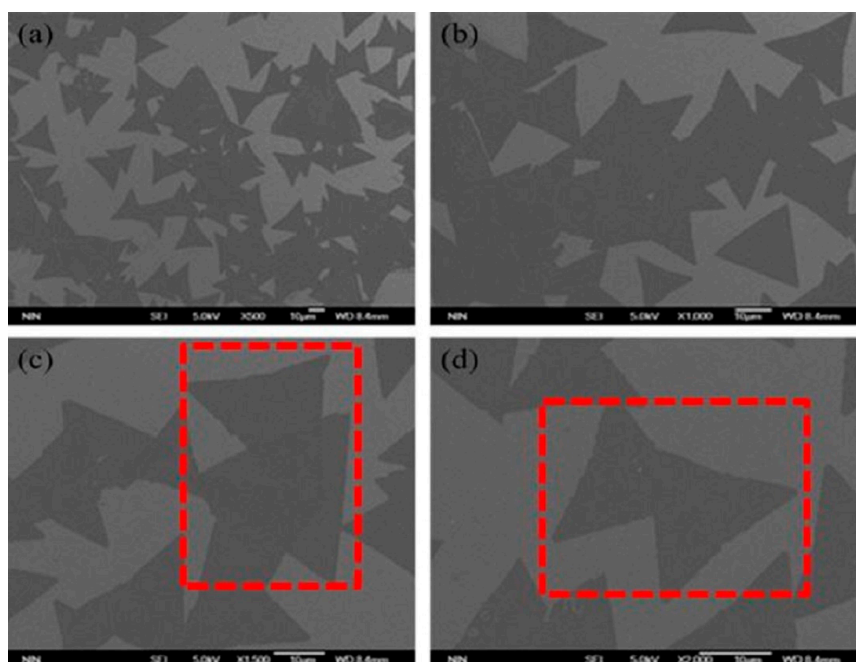


**Figure 3.** Field emission scanning electron microscope (FESEM) characterization of MoS<sub>2</sub>/WS<sub>2</sub> vertical hetero-junction at different magnifications (a) 500×; (b) 1000×; (c) 1500×; (d) 2000×.

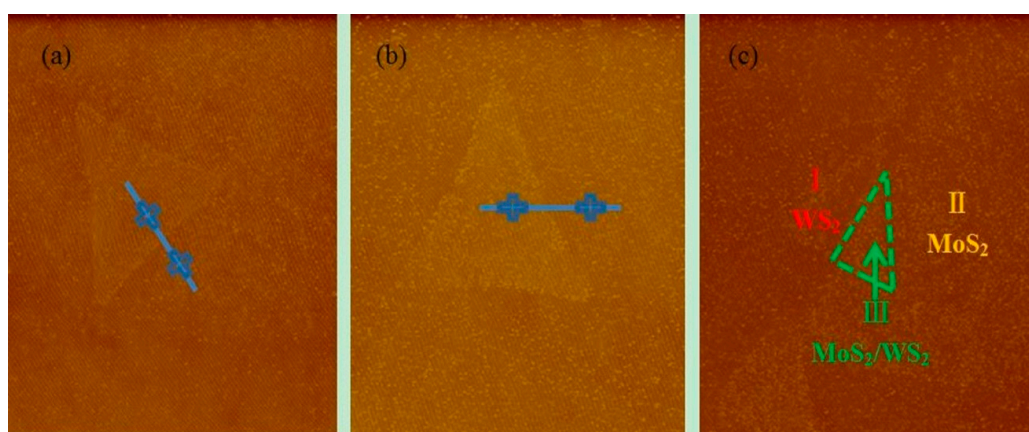


**Figure 4.** Atomic force microscope (AFM) image of (a) MoS<sub>2</sub>; (b) WS<sub>2</sub>; (c) MoS<sub>2</sub>/WS<sub>2</sub> vertical hetero-junction.

#### 4. Introduction and Analysis of the Spectrum Characteristics

Raman spectrum and PL spectrum have become the effective way to detect and identify the optical properties and layer number of MoS<sub>2</sub>, WS<sub>2</sub>, and MoS<sub>2</sub>/WS<sub>2</sub> vertical hetero-junction grown by the APCVD and dry transfer methods. The corresponding test characterizations require constant temperature and humidity, which are performed in an ultra-clean room environment.

##### 4.1. The Spectrum Characterization of Monolayer WS<sub>2</sub>

It can be found, by observing Figure 5a, that there are two characteristic peaks in the Raman spectrum of the WS<sub>2</sub> sample, and the peak positions of the E<sub>12g</sub> and A<sub>1g</sub> characteristic peaks are respectively located at 349 cm<sup>-1</sup> and 413 cm<sup>-1</sup>, which are fitted by the Gaussian function. The peak shift between two characteristic peaks decreases with the layer number decreases, which can be explained by the increase of the Van der Waals force. The Raman spectrums on the triangular WS<sub>2</sub> sample remain

consistent at different points, which can indicate that the sample is uniform. In Figure 5b, the strongest PL spectrum peak position of monolayer WS<sub>2</sub> is located at 636 nm. The band gap of monolayer WS<sub>2</sub> is calculated at 1.96 eV from the conversion relationship between the wavelength and electron volt, which is the same as the reported results. Besides, the PL spectrum also has an exciton peak of 2.04 eV. This is because the WS<sub>2</sub> sample has energy band splitting [23]. Figure 5c shows the Raman spectrum of monolayer WS<sub>2</sub> under the different laser powers. The Raman spectrum shape and relative position of the WS<sub>2</sub> sample move, to a certain extent, when the laser power increases. The Raman intensity of the E<sub>2g</sub><sup>1</sup> characteristic peak increases with laser power increase, and the E<sub>2g</sub><sup>1</sup> characteristic peak shape changes, especially when the laser power exceeds 10%. Meanwhile, the A<sub>1g</sub> characteristic peak intensity remains constant, but the position has a certain deviation. The PL spectrum intensity of the WS<sub>2</sub> sample strongest peak increases with a laser power increase, the strongest peak position is red-shifted, and the shape changes to some extent, as shown in Figure 5d. This phenomenon can be explained from two aspects here; on the one hand, higher power would generate more heat on the WS<sub>2</sub> sample, which has an effect on the power PL spectrum of WS<sub>2</sub>; on the other hand, the SiO<sub>2</sub>/Si substrate selected in the WS<sub>2</sub> growth experiment is an n-type doped semiconductor material [24].

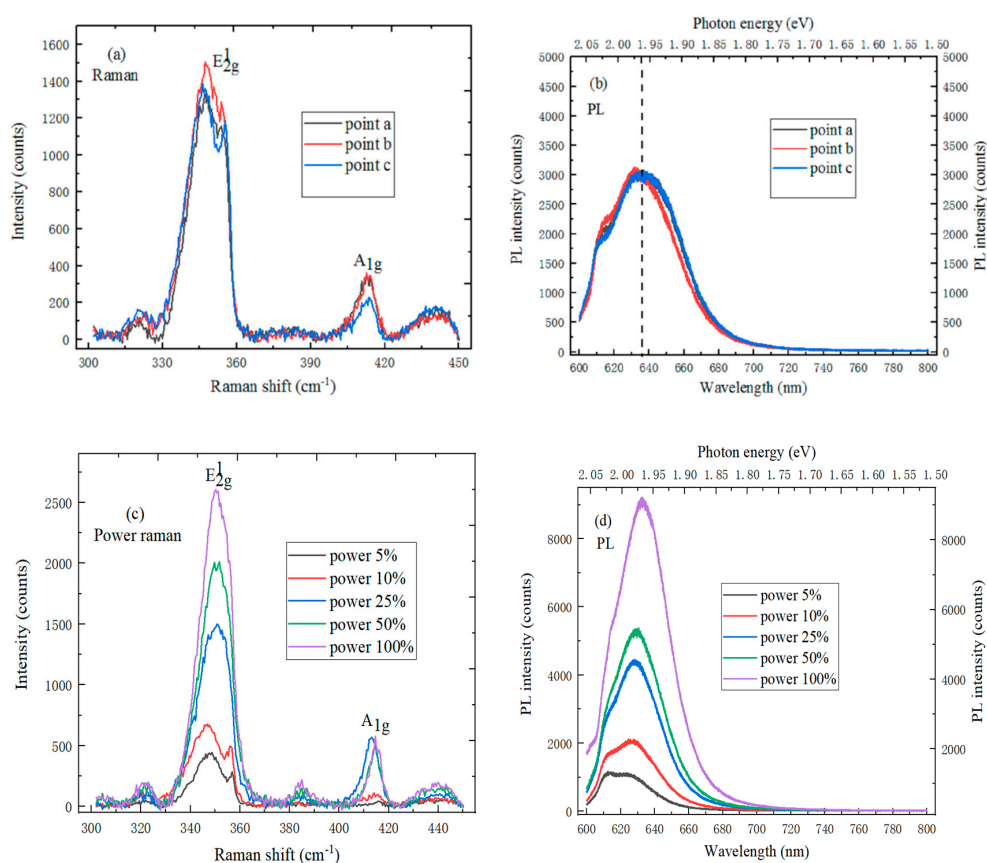


**Figure 5.** (a) The Raman spectrum and (b) Photoluminescence spectrum of monolayer WS<sub>2</sub> on SiO<sub>2</sub>/Si substrate at three different points; (c) Raman spectrum and (d) Photoluminescence spectrum of monolayer WS<sub>2</sub> on SiO<sub>2</sub>/Si Substrate under different laser powers.

#### 4.2. The Spectrum Characterization of Monolayer MoS<sub>2</sub>

In Figure 6a, the Raman spectrum of monolayer MoS<sub>2</sub> has two characteristic peaks, wherein the E<sub>2g</sub><sup>1</sup> characteristic peak is at 379 cm<sup>-1</sup>, the position of A<sub>1g</sub> characteristic peak is 398 cm<sup>-1</sup>, and the ratio of A<sub>1g</sub> to E<sub>2g</sub><sup>1</sup> characteristic peaks is approximately 1.051. Besides, the Raman spectrum intensity and position of the MoS<sub>2</sub> sample at different points are consistent, which shows that the monolayer MoS<sub>2</sub>

sample is highly uniform. It can be seen from Figure 6b that the strongest PL spectrum peak position of monolayer MoS<sub>2</sub> on SiO<sub>2</sub>/Si substrate is at 681.2 nm, and the electron volt is 1.82 eV, which is the same as the direct band gap width of monolayer MoS<sub>2</sub>. Besides, the PL spectrum of monolayer MoS<sub>2</sub> also has an exciton peak at 1.95 eV. The reason is that the Mo atom has 3d orbital electron interaction [25]. As shown in Figure 6c, the Raman spectrum intensity of MoS<sub>2</sub> sample increases when the laser power increases; the positions of E<sup>1</sup><sub>2g</sub> and A<sub>1g</sub> characteristic peaks are blue-shifted simultaneously, which is caused by the n-type doped semiconductor characteristics of SiO<sub>2</sub>/Si substrate [26]. Figure 6d shows the PL spectrum of monolayer MoS<sub>2</sub> under different laser powers. As the laser power increases, the strongest photoluminescence spectrum peak intensity of monolayer MoS<sub>2</sub> increases, and the shape and position of characteristic peaks do not change. It can be judged that MoS<sub>2</sub> on SiO<sub>2</sub>/Si substrate is monolayer, by characterizing and analyzing the Raman spectrum and photoluminescence spectrum of MoS<sub>2</sub>.

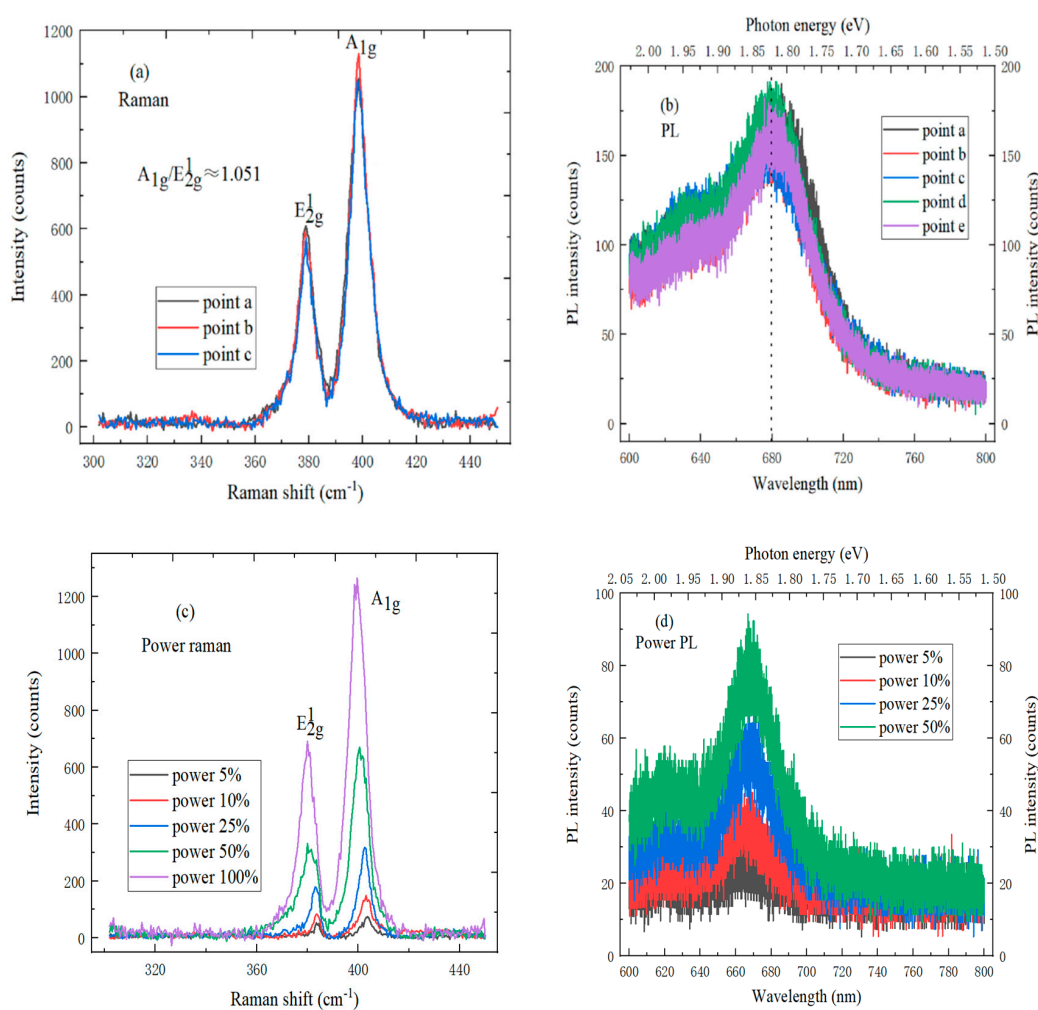


**Figure 6.** (a) Raman spectrum and (b) Photoluminescence (PL) spectrum of monolayer MoS<sub>2</sub> on SiO<sub>2</sub>/Si substrate at different points; (c) Raman spectrum and (d) PL spectrum of monolayer MoS<sub>2</sub> under different laser powers.

#### 4.3. Spectrum Characterization of the MoS<sub>2</sub>/WS<sub>2</sub> Heterojunction

The Raman spectrum of the MoS<sub>2</sub>/WS<sub>2</sub> hetero-junction is tested with the 532 nm laser excitation wavelength, to evaluate vibration characteristics and thickness. There are E<sup>1</sup><sub>2g</sub> and A<sub>1g</sub> Raman active modes in the Raman spectrum of MoS<sub>2</sub>/WS<sub>2</sub> hetero-junction, wherein the E<sup>1</sup><sub>2g</sub> is the in-plane optical mode that corresponds to the vibrational motion of Mo and S atoms in the x and y planes, while the

$A_{1g}$  is an out-of-plane vibration mode that corresponds to the vibrational motion of two S atoms along the z unit cell axis [27]. It can be found that four Raman characteristic peaks,  $WS_2-E_{2g}^1$ ,  $MoS_2-E_{2g}^1$ ,  $MoS_2-A_{1g}$ , and  $WS_2-A_{1g}$ , appeared in the  $MoS_2/WS_2$  hetero-junction region, and the corresponding peak positions are respectively located at  $350\text{ cm}^{-1}$ ,  $379\text{ cm}^{-1}$ ,  $398\text{ cm}^{-1}$  and  $413\text{ cm}^{-1}$ . In the four Raman peaks of  $MoS_2/WS_2$  hetero-junction, two peaks are the same as the Raman peaks of  $MoS_2$  film, and the other two peaks correspond to the Raman peaks of  $WS_2$  film. The four Raman peaks positions of  $MoS_2/WS_2$  hetero-junction did not show red or blue shift, which indicates that  $WS_2$  and  $MoS_2$  did not affect the long-distance Coulomb interaction between the effective charges [28]. The photoluminescence spectrum can be used to identify the band gaps of  $WS_2$  and  $MoS_2$ . Figure 7b shows the PL spectrum of  $WS_2/MoS_2$  hetero-junction under the 532 nm wavelength. The PL peak positions of  $WS_2$  and  $MoS_2$  are respectively located at 635 nm (1.96 eV) and 682 nm (1.82 eV), which is due to the direct exciton transition energy of bottom layer  $MoS_2$  and top layer  $WS_2$ . It can be seen by comparing and analyzing the PL spectrum of  $MoS_2/WS_2$  vertical hetero-junction and single  $MoS_2$  or  $WS_2$  thin films that the PL peak position of  $MoS_2/WS_2$  hetero-junction is the same as that of the single  $MoS_2$  or  $WS_2$  films, but the peak intensity of the  $MoS_2/WS_2$  hetero-junction is much lower than that of the single  $WS_2$  films, which can be caused by interlayer exciton relaxation. At the interface between  $MoS_2$  and  $WS_2$  composites, electrons from the conduction band of  $WS_2$  are transferred to the conduction band of  $MoS_2$ , and the holes from the valence band of  $MoS_2$  are moved to the valence band of  $WS_2$ , which would cause the separation of photo-generated electrons and holes [29]. A slight PL position shift and an additional weak peak of 1.82 eV can be observed in the epitaxial  $MoS_2/WS_2$  hetero-junction, which can be attributed to the recombination of spatially separated carriers. The two main factors of the PL spectrum quenching are the energy and charge transfer. In Figure 7c, the four characteristic peaks intensity of  $MoS_2/WS_2$  hetero-junction gradually increases with the laser power increase, wherein the  $E_{2g}^1$  and  $A_{1g}$  characteristic peak positions of bottom layer  $MoS_2$  are blue-shifted, and the  $A_{1g}$  characteristic peak position of top layer  $WS_2$  also shifted blue. Different laser powers on  $MoS_2/WS_2$  hetero-junction would generate different heat, which can affect the Raman spectrum of  $MoS_2/WS_2$  hetero-junction. The top layer  $WS_2$  may prevent the effective collection of Raman scattered signals from the bottom layer  $MoS_2$ . Meanwhile, the Raman signal from  $WS_2$  is also weakened when it passes the bottom layer of  $MoS_2$ , indicating that the bottom layer  $MoS_2$  can still affect the Raman intensity of the top layer  $WS_2$ . Figure 7d shows the photoluminescence spectrum of the  $MoS_2/WS_2$  hetero-junction under different laser powers. The strongest photoluminescence peak intensity of the  $MoS_2/WS_2$  hetero-junction increases with laser power increase; the strongest photoluminescence spectrum position red-shifted, and the strongest photoluminescence spectrum shape of  $MoS_2/WS_2$  hetero-junction also changes.

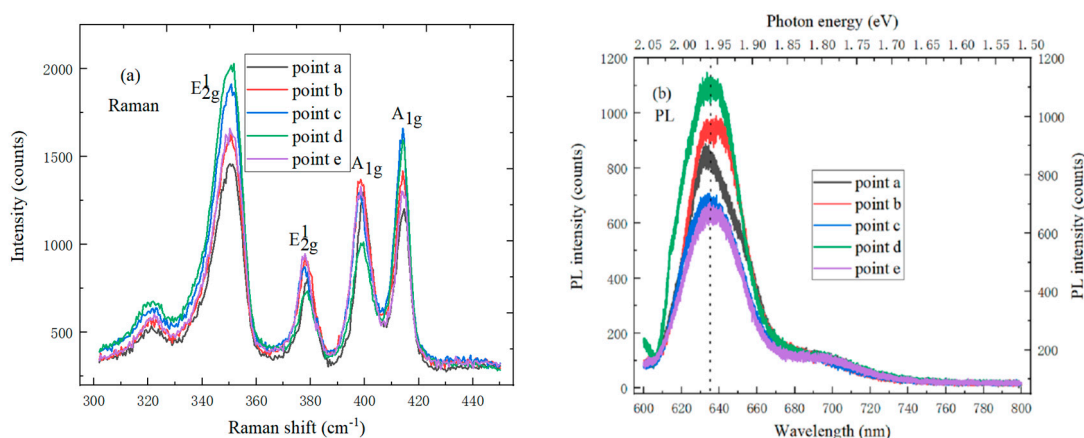
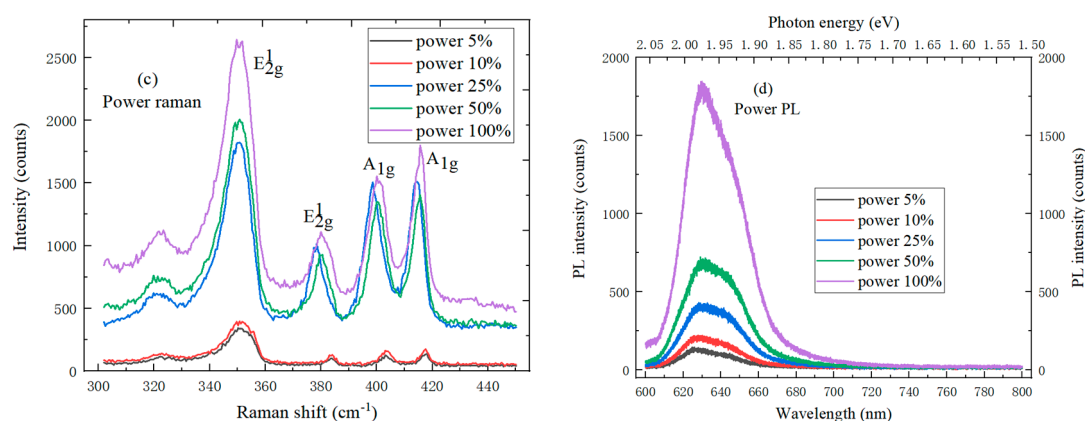


Figure 7. Cont.



**Figure 7.** (a) Raman spectrum and (b) PL spectrum of MoS<sub>2</sub>/WS<sub>2</sub> hetero-junction on SiO<sub>2</sub>/Si substrate at five points; (c) Power Raman spectrum and (d) Power photoluminescence spectrum of MoS<sub>2</sub>/WS<sub>2</sub> hetero-junction on SiO<sub>2</sub>/Si substrate.

## 5. Conclusions

The 2D TMDs materials have different energy band structures and band gaps, so that the physical properties of 2D TMDs materials can be finely adjusted by stacking with each other. The large-area, high-quality monolayer MoS<sub>2</sub> and WS<sub>2</sub> materials are first prepared by APCVD method in this paper. Then, the MoS<sub>2</sub>/WS<sub>2</sub> vertical hetero-junction is prepared by the dry transfer method, which can provide a well-defined interface between WS<sub>2</sub> and MoS<sub>2</sub> in the vertical dimension. The interface environment is the key factor affecting the performance of VDW hetero-structure modulation devices. The optimal reaction conditions of MoS<sub>2</sub>/WS<sub>2</sub> vertical hetero-junction by the APCVD and dry transfer methods are obtained through experiments. The composite materials are divided into the MoS<sub>2</sub>, WS<sub>2</sub> and MoS<sub>2</sub>/WS<sub>2</sub> hetero-junction regions, according to the morphology evolution of the MoS<sub>2</sub>/WS<sub>2</sub> vertical hetero-junction on the SiO<sub>2</sub>/Si substrate. Compared to the single MoS<sub>2</sub> or WS<sub>2</sub> materials, the PL spectrum characterization results show that the PL intensity of the MoS<sub>2</sub>/WS<sub>2</sub> hetero-junction is reduced by half, which is due to the effective photoelectron-hole separation phenomenon which occurred during the recombination process. Meanwhile, the strong interlayer coupling and effective interlayer charge transfer of the MoS<sub>2</sub>/WS<sub>2</sub> hetero-junction are systematically studied to strengthen the basic understanding of interlayer coupling, which can provide an unstructured and convenient method to explore the interface environment of the VDW hetero-structures. At the same time, the characterization results can help the mass production of various VDW hetero-junctions in future optoelectronic devices.

**Author Contributions:** Conceptualization and writing—original draft preparation, T.H.; methodology, S.W. and S.C.; validation, S.C. and K.Y.; writing—review and editing, H.L.; funding acquisition, H.L. All authors have read and agreed to the published version of the manuscript.

**Funding:** This research was funded by the National Natural Science Foundation of China (Grant No. U1866212 and 61904136), the Foundation for Fundamental Research of China (Grant No. JSZL2016110B003), the Major Fundamental Research Program of Shaanxi (Grant No. 2017ZDJC-26), the Innovation Foundation of Radiation Application (Grant No. KFZC2018040206). It was also supported by the Fundamental Research Funds for the Central Universities, and the Innovation Fund of Xidian University.

**Conflicts of Interest:** The authors declare no conflict of interest.

## References

1. Zhang, J.; Wang, J.; Chen, P.; Sun, Y.; Wu, S.; Jia, Z.; Lu, X.; Yu, H.; Chen, W.; Zhu, J.; et al. Observation of strong interlayer coupling in MoS<sub>2</sub>/WS<sub>2</sub> heterostructures. *Adv. Mater.* **2016**, *28*, 1950–1956. [[CrossRef](#)] [[PubMed](#)]

2. Zheng, J.; Yan, X.; Lu, Z.; Qiu, H.; Xu, G.; Zhou, X.; Wang, P.; Pan, X.; Liu, K.; Jiao, L. High-Mobility Multilayered MoS<sub>2</sub> Flakes with Low Contact Resistance Grown by Chemical Vapor Deposition. *Adv. Mater.* **2017**, *29*, 1604540. [[CrossRef](#)] [[PubMed](#)]
3. Zhang, W.; Huang, J.K.; Chen, C.H.; Chang, Y.H.; Cheng, Y.J.; Li, L.J. High gain phototransistors based on a CVD MoS<sub>2</sub> monolayer. *Adv. Mater.* **2013**, *25*, 3456–3461. [[CrossRef](#)] [[PubMed](#)]
4. Yang, P.; Yang, A.G.; Chen, L. Influence of seeding promoters on the properties of CVD grown monolayer molybdenum disulfide. *Nano Res.* **2019**, *12*, 823–827. [[CrossRef](#)]
5. Shin, G.H.; Koo, B.; Park, H.; Woo, Y.; Lee, J.E.; Choi, S.Y. Vertical-tunnel field-effect transistor based on a silicon–MoS<sub>2</sub> Three-dimensional–two-dimensional heterostructure. *ACS Appl. Mater. Interfaces* **2018**, *10*, 40212–40218. [[CrossRef](#)] [[PubMed](#)]
6. Wang, J.; Yao, Q.; Huang, C.W.; Zou, X.; Liao, L.; Chen, S.; Fan, Z.; Zhang, K.; Wu, W.; Xiao, X.; et al. High mobility MoS<sub>2</sub> transistor with low schottky barrier contact by using atomic thick h-BN as a tunneling layer. *Adv. Mater.* **2016**, *28*, 8302–8308. [[CrossRef](#)]
7. Yu, W.J.; Liu, Y.; Zhou, H.; Yin, A.; Li, Z.; Huang, Y.; Duan, X. Highly efficient gate-tunable photocurrent generation in vertical heterostructures of layered materials. *Nat. Nanotechnol.* **2013**, *8*, 952. [[CrossRef](#)]
8. Miao, J.; Hu, W.; Jing, Y.; Luo, W.; Liao, L.; Pan, A.; Wu, S.; Cheng, J.; Chen, X.; Lu, W. Surface plasmon-enhanced photodetection in few layer MoS<sub>2</sub> phototransistors with Au nanostructure arrays. *Small* **2015**, *11*, 2392–2398. [[CrossRef](#)]
9. Chen, J.; Zhao, X.; Tan, S.J.; Xu, H.; Wu, B.; Liu, B.; Fu, D.; Fu, W.; Geng, D.; Liu, Y.; et al. Chemical vapor deposition of large-size monolayer MoSe<sub>2</sub> crystals on molten glass. *J. Am. Chem. Soc.* **2017**, *139*, 1073–1076. [[CrossRef](#)]
10. Liu, K.; Zhang, L.; Cao, T.; Jin, C.; Qiu, D.; Zhou, Q.; Zettl, A.; Yang, P.; Louie, S.G.; Wang, F. Evolution of interlayer coupling in twisted molybdenum disulfide bilayers. *Nat. Commun.* **2014**, *5*, 4966. [[CrossRef](#)]
11. Moriya, R.; Yamaguchi, T.; Inoue, Y.; Morikawa, S.; Sata, Y.; Masubuchi, S.; Machida, T. Large current modulation in exfoliated-graphene/MoS<sub>2</sub>/metal vertical heterostructures. *Appl. Phys. Lett.* **2014**, *105*, 083119. [[CrossRef](#)]
12. Lee, C.; Yan, H.; Brus, L.E.; Heinz, T.F.; Hone, J.; Ryu, S. Anomalous lattice vibrations of single-and few-layer MoS<sub>2</sub>. *ACS Nano* **2010**, *4*, 2695–2700. [[CrossRef](#)]
13. Yu, H.; Liao, M.; Zhao, W.; Liu, G.; Zhou, X.J.; Wei, Z.; Zhou, S. Wafer-scale growth and transfer of highly-oriented monolayer MoS<sub>2</sub> continuous films. *ACS Nano* **2017**, *11*, 12001–12007. [[CrossRef](#)]
14. Zhao, Y.; Luo, X.; Li, H.; Zhang, J.; Araujo, P.T.; Gan, C.K.; Wu, J.; Zhang, H.; Quek, S.Y.; Dresselhaus, M.S.; et al. Interlayer breathing and shear modes in few-trilayer MoS<sub>2</sub> and WSe<sub>2</sub>. *Nano Lett.* **2013**, *13*, 1007–1015. [[CrossRef](#)] [[PubMed](#)]
15. Yang, W.; Chen, G.; Shi, Z.; Liu, C.C.; Zhang, L.; Xie, G.; MCheng Wang, D.; Yang, R.; Shi, D.; Watanabe, K.; et al. Epitaxial growth of single-domain graphene on hexagonal boron nitride. *Nat. Mater.* **2013**, *12*, 792. [[CrossRef](#)]
16. Shi, Y.; Zhou, W.; Lu, A.Y.; Fang, W.; Lee, Y.H.; Hsu, A.L.; Kim, S.M.; Kim, K.K.; Yang, H.Y.; Li, L.J.; et al. van der Waals epitaxy of MoS<sub>2</sub> layers using graphene as growth templates. *Nano Lett.* **2012**, *12*, 2784–2791. [[CrossRef](#)]
17. Zafar, A.; Nan, H.; Zafar, Z.; Wu, Z.; Jiang, J.; You, Y.; Ni, Z. Probing the intrinsic optical quality of CVD grown MoS<sub>2</sub>. *Nano Res.* **2017**, *10*, 1608–1617. [[CrossRef](#)]
18. Chow, P.K.; Singh, E.; Viana, B.C.; Gao, J.; Luo, J.; Li, J.; Lin, Z.; Elías, A.L.; Shi, Y.; Wang, Z. Wetting of mono and few-layered WS<sub>2</sub> and MoS<sub>2</sub> films supported on Si/SiO<sub>2</sub> substrates. *ACS Nano* **2015**, *9*, 3023–3031. [[CrossRef](#)] [[PubMed](#)]
19. Wen, Y.N.; Xia, M.G.; Zhang, S.L. Size effect on the magnetic and electronic properties of the monolayer lateral hetero-junction WS<sub>2</sub>-MoS<sub>2</sub> nanoribbon. *Appl. Surf. Sci.* **2016**, *371*, 376–382. [[CrossRef](#)]
20. Xu, W.; Li, S.; Zhou, S.; Lee, J.K.; Wang, S.; Sarwat, S.G.; Wang, X.; Bhaskaran, H.; Pasta, M.; Warner, J.H. Large Dendritic Monolayer MoS<sub>2</sub> Grown by Atmospheric Pressure Chemical Vapor Deposition for Electrocatalysis. *ACS Appl. Mater. Interfaces* **2018**, *10*, 4630–4639. [[CrossRef](#)] [[PubMed](#)]
21. Li, X.; Li, X.; Zang, X.; Zhu, M.; He, Y.; Wang, K.; Xie, D.; Zhu, H. Role of hydrogen in the chemical vapor deposition growth of MoS<sub>2</sub> atomic layers. *Nanoscale* **2015**, *7*, 8398–8404. [[CrossRef](#)] [[PubMed](#)]

22. Lopez-Sanchez, O.; Alarcon Llado, E.; Koman, V.; Fontcuberta i Morral, A.; Radenovic, A.; Kis, A. Light generation and harvesting in a van der Waals heterostructure. *ACS Nano* **2014**, *8*, 3042–3048. [[CrossRef](#)] [[PubMed](#)]
23. Lee, G.-H.; Yu, Y.-J.; Cui, X.; Petrone, N.; Lee, C.-H.; Choi, M.S.; Lee, D.-Y.; Lee, C.; Yoo, W.J.; Watanabe, K. Flexible and transparent MoS<sub>2</sub> field-effect transistors on hexagonal boron nitride-graphene heterostructures. *ACS Nano* **2013**, *7*, 7931–7936. [[CrossRef](#)] [[PubMed](#)]
24. Kaasbjerg, K.; Thygesen, K.S.; Jacobsen, K.W. Phonon-limited mobility in n-type single-layer MoS<sub>2</sub> from first principles. *Phys. Rev. B* **2012**, *85*, 115317. [[CrossRef](#)]
25. Chae, W.H.; Cain, J.D.; Hanson, E.D.; Murthy, A.A.; Dravid, V.P. Substrate-induced strain and charge doping in CVD-grown monolayer MoS<sub>2</sub>. *Appl. Phys. Lett.* **2017**, *111*, 143106. [[CrossRef](#)]
26. Frisenda, R.; Niu, Y.; Gant, P.; Molina-Mendoza, A.J.; Schmidt, R.; Bratschitsch, R.; Liu, J.; Fu, L.; Dumcenco, D.; Kis, A. Micro-reflectance and transmittance spectroscopy: A versatile and powerful tool to characterize 2D materials. *J. Phys. D Appl. Phys.* **2017**, *50*, 074002. [[CrossRef](#)]
27. Heo, H.; Sung, J.H.; Jin, G.; Ahn, J.H.; Kim, K.; Lee, M.J.; Jo, M.H. Rotation-Misfit-Free Heteroepitaxial Stacking and Stitching Growth of Hexagonal Transition-Metal Dichalcogenide Monolayers by Nucleation Kinetics Controls. *Adv. Mater.* **2015**, *27*, 3803–3810. [[CrossRef](#)]
28. Zhang, X.; Han, W.P.; Wu, J.B.; Milana, S.; Lu, Y.; Li, Q.Q.; Li, A.C.; Ferrari, P.H.; Tan, P.H. Raman spectroscopy of shear and layer breathing modes in multilayer MoS<sub>2</sub>. *Phys. Rev. B* **2013**, *87*, 115413. [[CrossRef](#)]
29. Lui, C.H.; Ye, Z.; Ji, C.; Chiu, K.C.; Chou, C.T.; Andersen, T.I.; Andersen, C.; Means-Shively, H.; Anderson, J.M.; Wu, T.; et al. Observation of interlayer phonon modes in van der Waals heterostructures. *Phys. Rev. B* **2015**, *91*, 165403. [[CrossRef](#)]

**Sample Availability:** Samples of the compounds MoS<sub>2</sub>/WS<sub>2</sub> vertical hetero-junction..... are available from the authors.



© 2020 by the authors. Licensee MDPI, Basel, Switzerland. This article is an open access article distributed under the terms and conditions of the Creative Commons Attribution (CC BY) license (<http://creativecommons.org/licenses/by/4.0/>).